ACSNANO www.acsnano.org

ARTICLE

Engineering Chimeric Receptors To Investigate the Size- and Rigidity-Dependent Interaction of PEGylated Nanoparticles with Cells

Wei-Chiao Huang,[†,¶] Pierre-Alain Burnouf,[†,‡,¶] Yu-Cheng Su,[†] Bing-Mae Chen,[†] Kuo-Hsiang Chuang,[§] Chia-Wei Lee,[∥] Pei-Kuen Wei,[∥] Tian-Lu Cheng,[*,⊥] and Steve R. Roffler[*,†]

[†]Institute of Biomedical Science, Academia Sinica, Taipei 11529, Taiwan

[‡]Taiwan International Graduate Program in Molecular Medicine, National Yang-Ming University and Academia Sinica, Taipei, Taiwan

[§]Graduate Institute of Pharmacognosy, Taipei Medical University, Taipei 110, Taiwan

[∥]Research Center for Applied Sciences, Academia Sinica, Taipei 11529, Taiwan

[⊥]Department of Biomedical and Environmental Biology, Center for Biomarkers and Biotech Drugs, Kaohsiung Medical University, Kaohsiung 80708, Taiwan

Supporting Information

ABSTRACT: **Attachment of ligands to the surface of nanoparticles (NPs) is an attractive approach to target specific cells and increase intracellular delivery of nanocargos. To expedite investigation of targeted NPs, we engineered human cancer cells to express chimeric receptors that bind polyethylene glycol (PEG) and internalize stealth NPs in a fashion similar to ligand-targeted liposomes against epidermal growth factor receptor 1 or 2 (HER1 or HER2), which are validated targets for cancer therapy. Measurement of the rate of endocytosis and lysosomal accumulation of small (80−94 nm) or large (180−220 nm) flexible liposomes or more rigid lipid-coated mesoporous silica particles in human HT29 colon cancer and SKBR3 breast cancer cells that express chimeric receptors revealed that larger and more rigid NPs were internalized more slowly than smaller and more flexible NPs. An exception is when both the small and large liposomes underwent endocytosis *via* HER2. HER1 mediated faster and greater uptake of NPs into cells but retained NPs less well as compared to HER2. Lysosomal accumulation of NPs internalized *via* HER1 was unaffected by NP rigidity but was inversely related to NP size, whereas large rigid NPs internalized by HER2 displayed increased lysosomal accumulation. Our results provide insight into the effects of NP properties on receptor-mediated endocytosis and suggest that anti-PEG chimeric receptors may help accelerate investigation of targeted stealth NPs.**

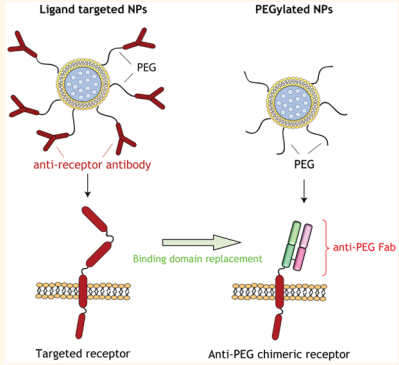

KEYWORDS: *PEGylated liposomes, immunoliposomes, αPEG antibody, polyethylene glycol, HER1, HER2, clathrin-mediated endocytosis, caveolin, stealth NPs*

Nanoparticles (NPs) are increasingly under investigation for delivering therapeutic agents to tumors. NP accumulation in tumors is controlled by the enhanced permeability and retention (EPR) effect in which nanosized particles can pass through leaky blood vessels and accumulate in the tumor interstitial space.[1] Most therapeutic agents, however, must enter individual cancer cells to reach their appropriate molecular target for effective anticancer activity. Attachment of ligands on the surface of NPs can increase interactions with specific cellular receptors and promote receptor-mediated endocytosis of the NPs (Figure 1A), thereby increasing cellular uptake of the therapeutic cargo with concomitant enhancement of antitumor activity.[2−6]

NP efficacy can be greatly affected by the rate of cellular uptake and the intracellular fate of the nanocargos. Thus, many studies have investigated the cellular uptake of nontargeted NPs.[7−10] By contrast, the relationship between NP physiochemical properties, cellular uptake, and intracellular routing is less well understood for ligand-targeted NPs. It is clear, however, that NP properties such as size and shape can greatly alter the receptor-mediated endocytosis and cellular response of ligand-targeted NPs.[9,11] Therefore, it is important to under-

Received: September 9, 2015
Accepted: January 7, 2016
Published: January 7, 2016

DOI: 10.1021/acsnano.5b05661
ACS Nano 2016, 10, 648−662

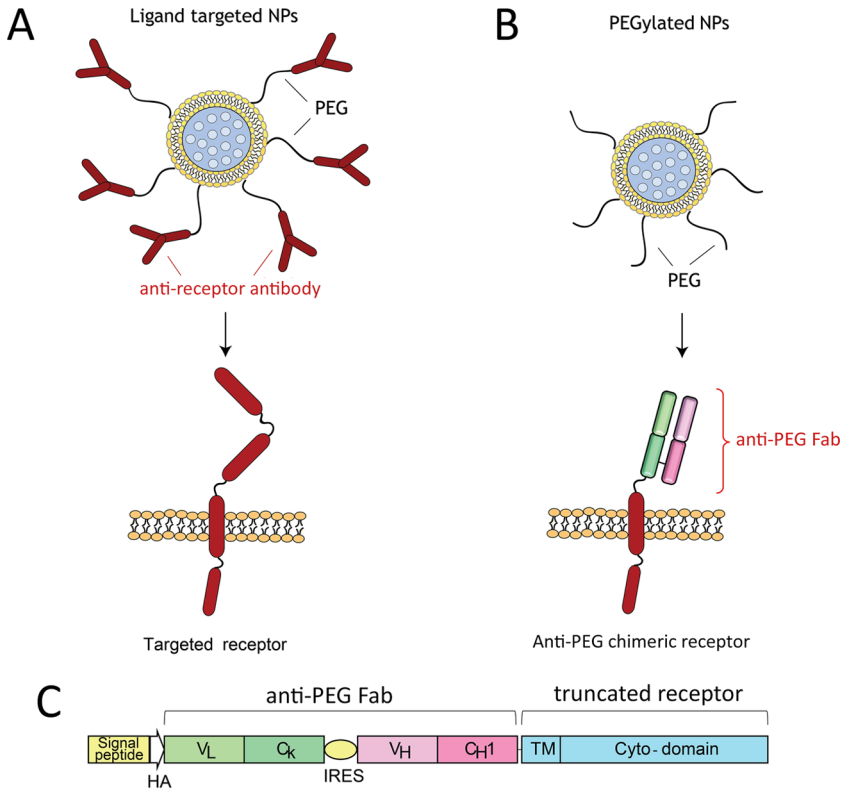

Figure 1. Illustration, construction, and expression of functional αPEG chimeric receptors. (A) Illustration of antibody-targeted NPs that can bind and internalize into cancer cells *via* endogenous receptors on the cell membrane. (B) PEGylated NPs can bind and internalize into cancer cells that have been engineered to express anti-PEG chimeric receptors. The chimeric receptors have an extracellular domain (anti-PEG Fab) that can bind to PEGylated NPs. The anti-PEG Fab is fused to the transmembrane and cytosolic domains of a membrane receptor expressed on cancer cells (*i.e.*, HER1 or HER2) that may mediate endocytosis and intracellular routing in a similar fashion as the endogenous cell receptors. (C) Anti-PEG chimeric receptor genes include an immunoglobulin signal peptide, an HA epitope tag, an anti-PEG Fab fragment, and the transmembrane and cytosolic domains of a cancer cell receptor, such as HER1 or HER2. V_L, light chain variable domain; Cκ, light chain kappa domain; V_H, heavy chain variable domain; C_H1, heavy chain first constant domain; TM, transmembrane domain of HER1 or HER2; Cyto-domain, cytoplasmic tail of HER1 or HER2.

stand how NP properties affect the uptake, routing, and therapeutic activity of targeted nanocarriers.

An important obstacle to the systematic investigation of targeted NPs is the increased level of complexity involved in their production. It can be time-consuming and expensive to generate a panel of targeted NPs, which involves preparation and purification of a targeting ligand such as a monoclonal antibody fragment, chemical conjugation of the ligand to the NPs, and subsequent validation that NP and ligand properties and activities were not deleteriously altered. Moreover, it is difficult to ensure that all NPs possess similar densities and activities of the targeting ligand, which could alter their binding affinity[12] and rate of internalization.[13] These issues have hindered the careful comparison of different NPs targeting the same receptor.

Here we investigated an alternative approach to advance the investigation and development of targeted NPs by diminishing reliance on ligand preparation and surface conjugation of NPs. Cancer cells were developed that stably express chimeric receptors that can directly bind to unliganded NPs, yet act as cellular receptors for uptake and intracellular routing of the NPs (Figure 1B). The receptors were composed of two parts: an extracellular domain that can bind to NPs (anti-PEG Fab) and a truncated cellular receptor that directs the endocytosis of the NPs into cancer cells (Figure 1C).[14] We predicted that the engineered receptors could bind untargeted NPs and induce receptor-mediated uptake into cancer cells in a fashion that recapitulates ligand-targeted NPs that bind to the corresponding natural receptor on the cells. Successful creation of cell lines that express chimeric receptors might then allow systematic development, comparison, and investigation of targeted NPs without the need to covalently attach targeting ligands to the NPs.

We choose to use antibody fragments that can bind to polyethylene glycol (PEG) for the NP binding domain of the chimeric receptors. PEG is a nontoxic and non-antigenic biocompatible polymer that is often used to create "stealth" NPs that display decreased uptake by macrophages in the liver and enhanced uptake into the tumor interstitial space by the EPR effect.[15−17] The common use of PEG in NP fabrication makes this a useful handle for NP recognition by the chimeric receptors. HER1 and HER2 were selected in our study as the other half of the chimeric receptors. These membrane receptors are overexpressed in several tumor types and are clinical targets for both drug and antibody therapy.[18−25] Several NPs that target HER1 or HER2 are also undergoing clinical trials such as MM-302, an immunoliposome that binds to HER2, and C225-ILsS-DOX, an immunoliposome that binds to HER1.[26,27] Chimeric receptors constructed from HER1 and HER2 are therefore relevant for investigation of targeted NPs.

In the present study, we sought to (1) engineer and express chimeric receptors that could bind stealth NPs on cancer cells,

DOI: 10.1021/acsnano.5b05661
ACS Nano 2016, 10, 648−662

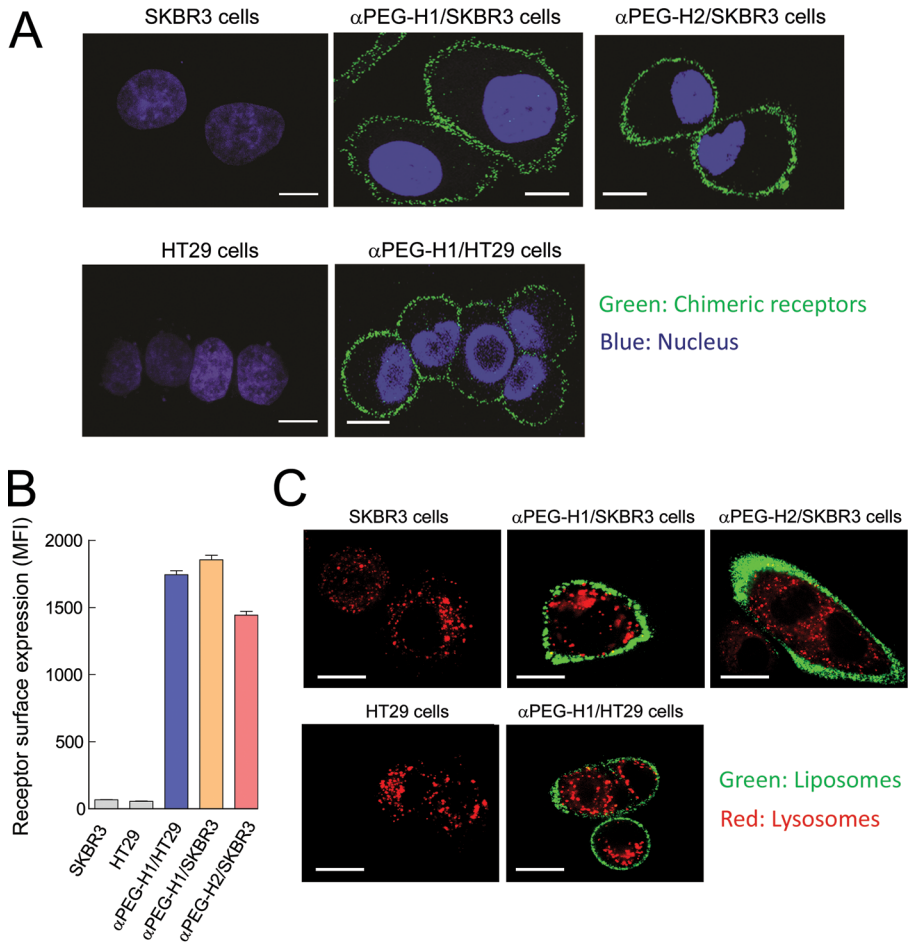

Figure 2. Chimeric receptors expressed on cancer cells can bind stealth liposomes. (A) Parental SKBR3 and HT29 cells, HT29 cells engineered to express chimeric αPEG-HER1 receptors (αPEG-H1/HT29 cells), or SKBR3 cells engineered to express chimeric αPEG-HER1 or αPEG-HER2 receptors (αPEG-H1/SKBR3 and αPEG-H2/SKBR3 cells, respectively) on glass slides at 4 °C were immunofluorescence stained (green) for the HA epitope tag on the chimeric receptors. Nuclei were visualized by staining cells with Hoechst 33342 (blue). The cells were imaged on a confocal microscope. Scale bars = 20 μm. (B) Indicated cells were immunofluorescence stained for the HA epitope tag on chimeric receptors (green) at 4 °C, and then the mean fluorescence intensity of viable cells was determined by FACS (n = 3), bars, SD. (C) Parental HT29 and SKBR3 cells or cells engineered to express chimeric receptors on glass slides were stained with LysoTracker Red DND-99 to visualize lysosomes (red) and incubated with fluorescent PEGylated liposomes (green) for 15 min at 37 °C before the cells were imaged on a confocal microscope. Scale bars = 10 μm.

(2) assess whether the chimeric receptors could mimic endocytosis of NPs targeted to HER1 or HER2 on cancer cells, and (3) directly address how selected NP properties affect receptor-mediated endocytosis of targeted stealth NPs.

RESULTS AND DISCUSSION

Surface Expression of Functional HER1 and HER2 Chimeric Receptors. Chimeric HER1 and HER2 receptors were constructed by fusing an anti-PEG Fab fragment to truncated HER1 or HER2 receptors (Figure 1C). The anti-PEG Fab is designed to bind to stealth NPs, whereas the HER1 and HER2 portions of the receptors are included to trigger receptor-mediated endocytosis of the NPs. HT29 colon cancer cells that stably express chimeric HER1 receptors (αPEG-H1/HT29) and SKBR3 breast cancer cells that express chimeric HER1 or HER2 receptors (αPEG-H1/SKBR3 and αPEG-H2/SKBR3 cells, respectively) were generated by retroviral transduction of the chimeric receptor genes and drug selection of stable cell lines. Expression of the chimeric receptors on cells was first evaluated by confocal microscopy using an antibody to detect the HA epitope tag present at the amino-terminus of the receptors. Confocal imaging demonstrated membrane expression of αPEG-H1 or αPEG-H2 receptors on engineered SKBR3 and HT29 cell lines (Figure 2A). Quantification of the levels of the chimeric receptors on the cell lines as determined by fluorescence-activated cell sorting (FACS) showed that high levels of αPEG-H1 were present on αPEG-H1/SKBR3 cells and αPEG-H1/HT29 cells, and slightly lower levels of αPEG-H2 were present on αPEG-H2/SKBR3 cells (Figure 2B). Confocal imaging showed that PEGylated liposomes labeled with the fluorescent dye DiIC18(5) bound to the surface of αPEG-H1/HT29, αPEG-H1/SKBR3, and αPEG-H2/SKBR3 cells but not to the parental cells (Figure 2C). The fluorescent dye was stably retained in liposomes for at least 5 h in culture medium containing serum (Figure S1).

Chimeric Receptors Can Mediate NP Endocytosis. To investigate if the chimeric receptors could mimic the cellular behavior of targeted liposomes, we first made immunoliposomes that can target HER1 or HER2 on cancer cells (Figure 3A). Single-chain antibodies (scFv) against HER1 and HER2 were generated with a C-terminal His-tag for affinity purification and a cysteine residue for covalent attachment to

DOI: 10.1021/acsnano.5b05661
ACS Nano 2016, 10, 648–662

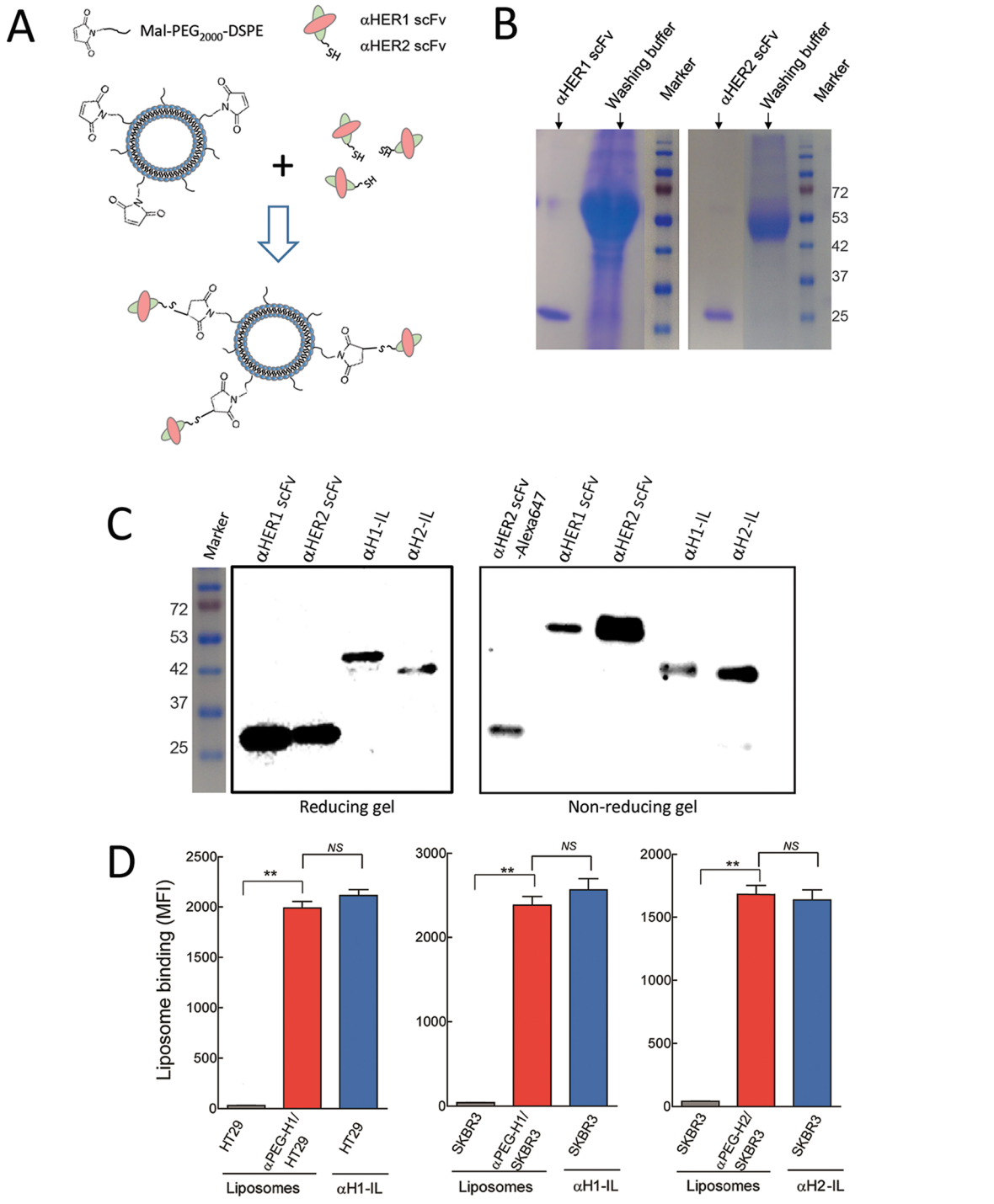

Figure 3. Immunoliposome and PEG-liposome binding to cells. (A) αH1-IL and αH2-IL immunoliposomes were prepared by covalent reaction of a sulfhydryl group at the C-terminus of αHER1 or αHER2 scFv with lipid−PEG−maleimide molecules on the liposomes. (B) SDS-PAGE showing the purified αHER1 and αHER2 scFv. Wash shows the flow through from the Co^{2+} TALON Superflow columns. (C) Immunoblot detection of scFv under reducing conditions (left panel) or nonreducing conditions (right panel). The scFv is present as disulfide-linked dimers under nonreducing conditions. Anti-HER2 scFv linked to Alexa Fluor 647 (αHER2 scFv-Alexa647), and scFv linked to lipid−PEG−maleimide molecules (αH1-IL and αH2-IL) on the immunoliposomes is also shown. (D) Parental cells and cells expressing chimeric receptors were incubated with fluorescent PEGylated liposomes. Parental cells were also incubated with αH1-IL or αH2-IL immunoliposomes and analyzed by FACS to assess binding of the liposomes to the cells. Results show MFI (n = 3), bars, SD, $^{**}p \leq 0.01$; NS, not significant.

liposomes. SDS-PAGE analysis of purified scFv demonstrated major bands with the expected molecular weights of approximately 25 kDa (Figure 3B). The scFv appeared to be monomers under reducing conditions (Figure 3C, left panel) but formed dimers under nonreducing conditions (Figure 3C, right panel), consistent with the presence of the C-terminal cysteine group. Reaction of a maleimide derivative of Alexa Fluor 647 to the C-terminal cysteine of αHER2 scFv prevented

DOI: 10.1021/acsnano.5b05661
ACS Nano 2016, 10, 648−662

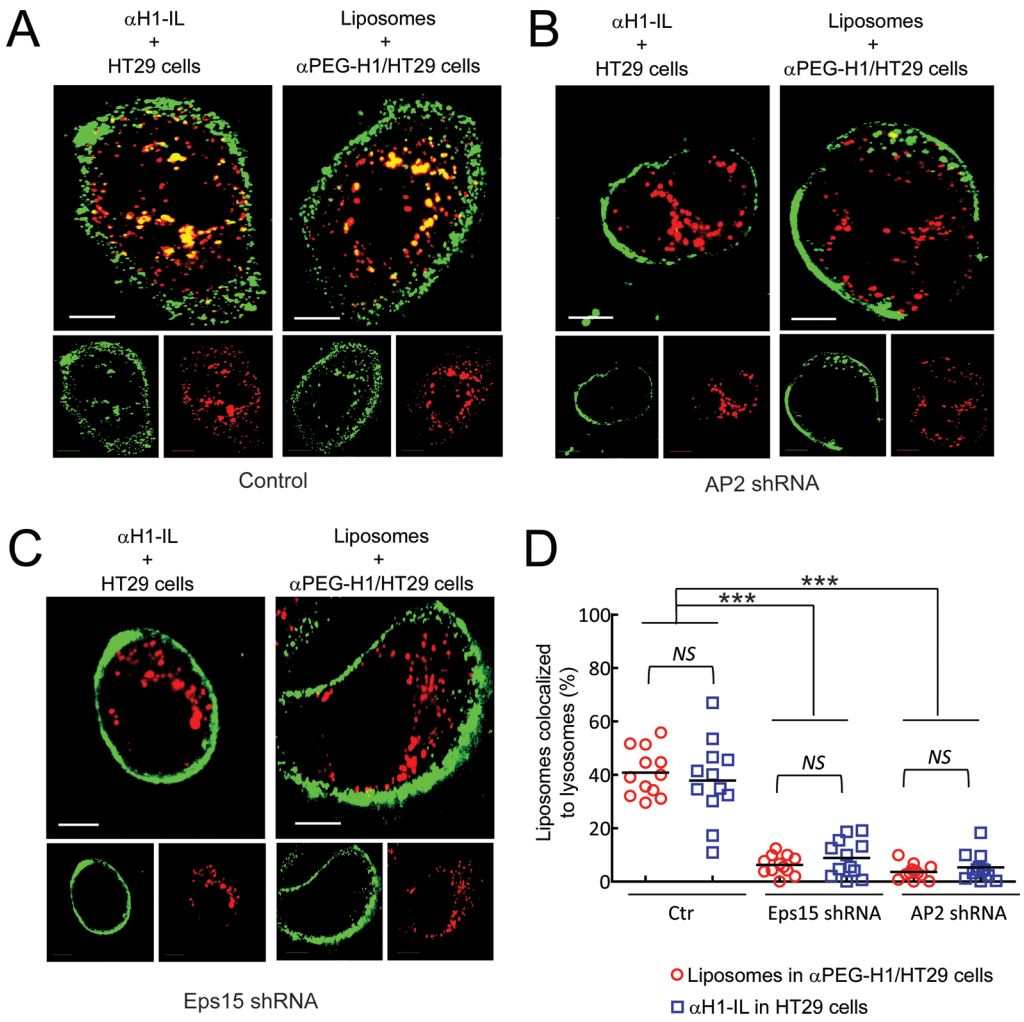

Figure 4. Comparison of lysosomal accumulation of PEGylated liposomes in αPEG-H1/HT29 cells and αH1-IL immunoliposomes in HT29 cells. (A) αH1-IL immunoliposomes were incubated with parental HT29 cells (left panel), and PEG-liposomes were incubated with αPEG-H1/HT29 cells (right panel) for 2 h at 37 °C. Confocal imaging of green liposomes, red lysosomes, and yellow colocalization of liposomes and lysosomes is shown. Scale bars = 10 μm. (B) Cells were treated with AP2 shRNA to inhibit clathrin-mediated endocytosis before incubation of the cells with liposomes as in (A). (C) Cells were treated with EPS15 shRNA to inhibit clathrin-mediated endocytosis before incubation of the cells with liposomes as in (A). (D) Percentage of the liposomes that colocalized with the red fluorescent lysosomal marker was quantified from confocal images of individual cells. The horizontal bars indicate mean colocalization percentages (n = 12). Significant differences between mean values are indicated; ***$p \leq 0.005$; NS, not significant.

dimer formation under nonreducing conditions (Figure 3C, αHER2 scFv-Alexa647), demonstrating the presence of a free sulfhydryl group in the scFv. Purified scFv was reacted with liposomes that incorporated lipid−PEG−maleimide molecules to generate immunoliposomes (αH1-IL or αH2-IL) that can bind to HER1 or HER2, respectively. SDS-PAGE followed by Western blotting demonstrated a shift in scFv size in αH1-IL and αH2-IL, corresponding to covalent attachment to lipid−PEG−maleimide molecules (Figure 3C). To verify functional binding of the ILs, we incubated nontargeted stealth liposomes with αPEG-H1/HT29, αPEG-H1/SKBR3, and αPEG-H2/SKBR3 cells, whereas αH1-IL or αH2-IL immunoliposomes were incubated with parental SKBR3 and HT29 cancer cells. HT29 cells express HER1, whereas SKBR2 cells express both HER1 and HER2 (Figure S2).[28] FACS analysis of liposome fluorescence on the cells revealed comparable binding of stealth liposomes to cells expressing HER1 or HER2 chimeric receptors and targeted immunoliposomes binding to the parental cells (Figure 3D). For example, PEGylated liposome binding to αPEG-H1/HT29 cells was not significantly different from the binding of αH1-IL immunoliposomes to HT29 cells. As expected, the untargeted stealth liposomes bound poorly to parental HT29 and SKBR3 cells. We conclude that the chimeric receptors expressed on HT29 and SKBR3 cells could bind PEGylated liposomes at levels that were comparable to the binding of targeted immunoliposomes to their corresponding receptors on HT29 and SKBR3 cells.

We next sought to test if chimeric HER1 and HER2 receptors could mediate the endocytosis of NPs into cancer cells in a qualitatively similar fashion as the corresponding endogenous membrane receptors. Liposomes labeled with DiIC18(5) were incubated for 2 h at 37 °C with αPEG-H1/HT29 and parental HT29 cells previously treated with LysoTracker Red DND99 to visualize lysosomes. Overlap of green and red signals to produce yellow indicates colocalization of liposomes (green) and lysosomes (red) as visualized under a confocal microscope. We observed a similar pattern of liposomes accumulating in the lysosomal compartment for

DOI: 10.1021/acsnano.5b05661
ACS Nano 2016, 10, 648−662

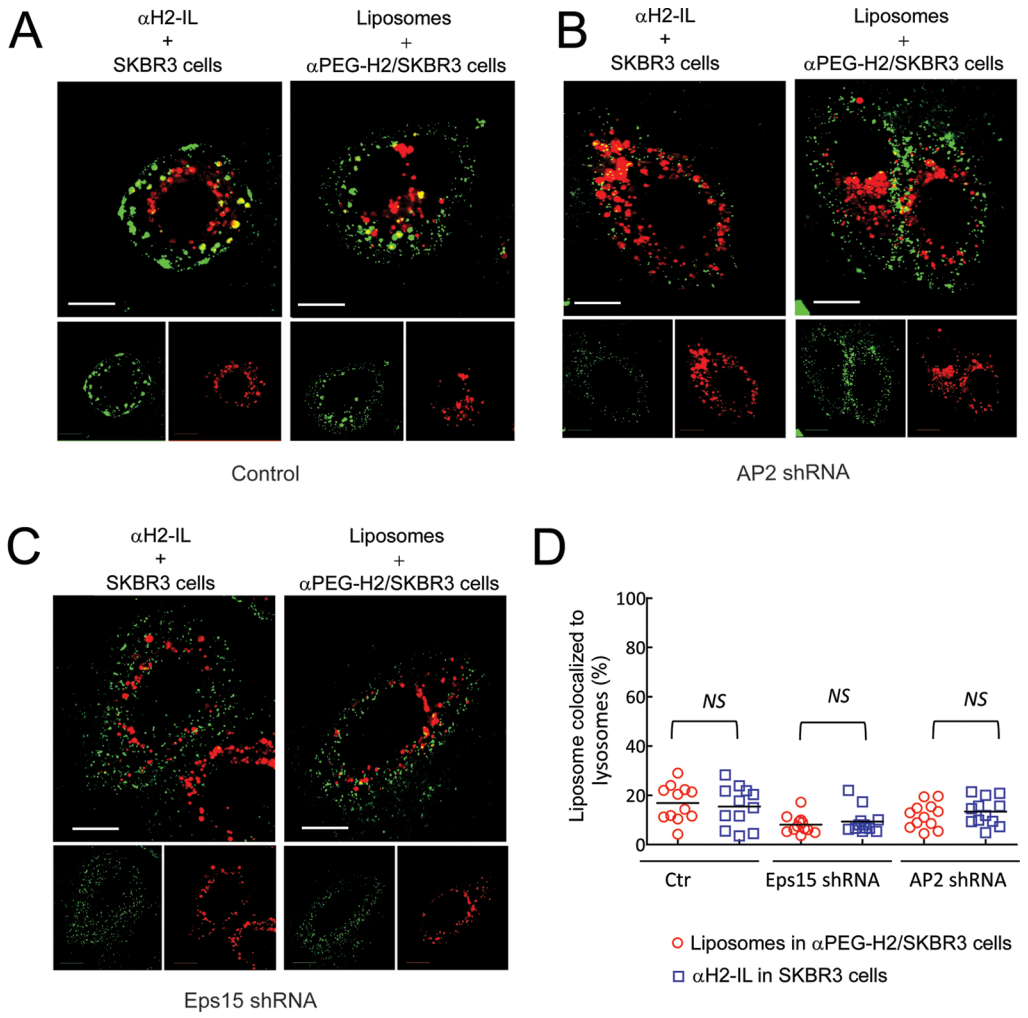

Figure 5. Comparison of lysosomal accumulation of PEGylated liposomes in αPEG-H2/SKBR3 cells and αH2-IL immunoliposomes in SKBR3 cells. (A) αH2-IL immunoliposomes were incubated with parental SKBR3 cells (left panel), while PEG-liposomes were incubated with αPEG-H2/SKBR3 cells (right panel) for 2 h at 37 °C. Confocal imaging of green liposomes, red lysosomes, and yellow colocalization of liposomes and lysosomes is shown. Scale bars = 10 μm. (B) Cells were treated with AP2 shRNA to inhibit clathrin-mediated endocytosis before incubation of the cells with liposomes as in (A). (C) Cells were treated with EPS15 shRNA to inhibit clathrin-mediated endocytosis before incubation of the cells with liposomes as in (A). (D) Percentage of the liposomes that colocalized with red fluorescent lysosomal marker was quantified from confocal images of individual cells. The horizontal bars indicate mean colocalization percentages (*n* = 12). Significant differences between mean values are indicated; NS, not significant.

PEGylated liposomes in αPEG-H1/HT29 cells and αH1-IL in HT29 cells (Figure 4A). Quantification of lysosomal accumulation of the NPs in lysosomes showed no significant difference of PEG-liposomes in αPEG-H1/HT29 cells (40.8% of liposomes colocalized to lysosomes) as compared to αH1-IL in HT29 cells (38.8% of liposomes colocalized to lysosomes) (Figure 4D).

Ligand binding to HER1 can stimulate clathrin-mediated endocytosis and routing to the lysosomal compartment of cells.[29] The AP2 adaptor complex and EGFR pathway substrate 15 (Eps15) are important for HER1-mediated endocytosis.[30,31] The AP2 adaptor complex is a heterotetrameric protein complex that interacts with membrane receptors and clathrin to form clathrin-coated vesicles.[32,33] Eps15 is constitutively associated with AP2 and is involved in formation of clathrin-coated vesicles and the endocytosis of HER1.[34] We therefore treated HT29 and αPEG-H1/HT29 cells with AP2 or Eps15 shRNA to knock down the expression of these molecules and impede HER1-mediated endocytosis. HT29 cells treated with AP2 or Eps15 shRNA displayed reduced internalization of αH1-IL (Figure 4B,C, left panels) and significantly less colocalization with lysosomal markers (Figure 4D) as compared to parental HT29 cells (6.3 and 3.6% for AP2 and Eps15 shRNA-treated cells *versus* 40.8% for untreated cells), consistent with reduced HER1-mediated endocytosis of the ligand-targeted liposomes. shRNA treatment also decreased the uptake of PEG-liposomes into αPEG-H1/HT29 cells (Figure 4B,C, right panels) and significantly reduced lysosome localization as compared with the same cells without shRNA treatment (Figure 4D) (8.8 and 5.3% for AP2 and Eps15 shRNA-treated cells *versus* 38.8% for untreated cells). These results indicate that chimeric HER1 receptors can mediate the endocytosis of untargeted stealth NPs in a qualitatively similar fashion as immunoliposomes targeted to HER1 in HT29 cells.

Ligand density on NPs can influence factors such as cell binding, uptake kinetics, and internalization efficiency.[35,36] Liposomes containing 2, 5, or 10% PEG–lipid (PEG–lipid/lipid, wt/wt) were prepared with similar fluorescent dye loading

DOI: 10.1021/acsnano.5b05661
ACS Nano 2016, 10, 648–662

(Figure S3A) to investigate the influence of PEG density on liposome internalization. The uptake of the liposomes, measured as internalized fluorescence in αPEG-H1/SKBR3 cells, was inversely related to PEG density on the liposomes with about 30% less uptake observed for liposomes coated with 10% PEG as compared to 2% PEG (Figure S3B). The reduced uptake appeared to be primarily related to lower binding of PEGylated liposomes containing high densities of PEG (Figure S3C).

We also compared the endocytosis of liposomes into cells *via* chimeric HER2 receptor or endogenous HER2 on SKBR3 cells. Two hours after addition of liposomes to cells, only low levels (16.9%) of αH2-IL colocalized with lysosomal markers in SKBR3 cells, similar to the levels of PEGylated liposomes that colocalized to the lysosomes (15.5%) in αPEG-H2/SKBR3 cells (Figure 5A,D). These results are consistent with previous studies showing that 20% of anti-HER2 antibody-conjugated NPs colocalized to lysosomes in SKBR3 and TD47 cells.[37] HER2-mediated endocytosis is believed to proceed *via* caveolae, which do not rely on AP2 or Eps15. Thus, αPEG-H2/SKBR3 cells treated with AP2 shRNA or Eps15 shRNA did not display large alterations in cellular uptake or lysosomal localization of PEGylated liposomes (Figure 5B–D) as compared with untreated αPEG-H2/SKBR3 cells (9.3 and 13.4% for AP2 or Eps15 shRNA-treated cells *versus* 15.5% for untreated cells). Importantly, there was no significant differences between the lysosomal accumulation of αH2-IL in SKBR3 cells and PEG-liposomes in αPEG-H2/SKBR3 cells under comparable conditions (Figure 5D) (8.1 and 11.7% for AP2 or Eps15 shRNA-treated SKBR3 cells *versus* 9.3 and 13.4% for AP2 or Eps15 shRNA-treated αPEG-H2/SKBR3 cells). Collectively, our data indicate that HER1 and HER2 chimeric receptors mediated similar patterns of endocytosis as the corresponding endogenous receptors.

Cellular Uptake *via* HER1 and HER2 Differentially Depends on the Size and Rigidity of NPs. We used cells that stably express HER1 and HER2 chimeric receptors to investigate how selected NP properties affect their cellular uptake and routing. PEGylated NPs were first prepared with different sizes and rigidities. Liposomes (more flexible) and lipid-coated mesoporous silica nanoparticles (MSN) (more rigid; L-MSN) with smaller or larger sizes were labeled with fluorescent DiIC18(5) dye. DiIC18(5), which is a lipophilic dye, was stably retained in liposomes and lipid-coated MSN for at least 5 h (Figure S1), indicating good NP stability and fluorescent dye retention. The average sizes of the PEGylated liposomes as measured by dynamic light scattering were 81 ± 2 nm (small) and 185 ± 2 nm (large), whereas the average size of the L-MSN were 94 ± 4 nm (small) and 220 ± 14 nm (large) (Figure 6A). PEG coating of the NPs was assessed by ELISA using anti-PEG antibodies for the capture and detection of the PEGylated NPs.[38] Based on equal concentrations of lipids added to the assay, we verified that PEG was present on each type of NP (Figure 6B). The amount of PEG on the liposomes was similar to the PEG density found on Doxisome, a commercial liposomal doxorubicin formulation. PEG levels on the L-MSN appeared to be slightly greater than on liposomes, likely due to sterically restricted enhanced display of PEG molecules on the outside face of the lipid bilayer in L-MSN.

The uptake of the PEGylated NPs into SKBR3 breast cancer cells that express HER1 and HER2 chimeric receptors was determined by incubating αPEG-H1/SKBR3 or αPEG-H2/SKBR3 cells with the various NPs for different times (0.5, 1, 2,

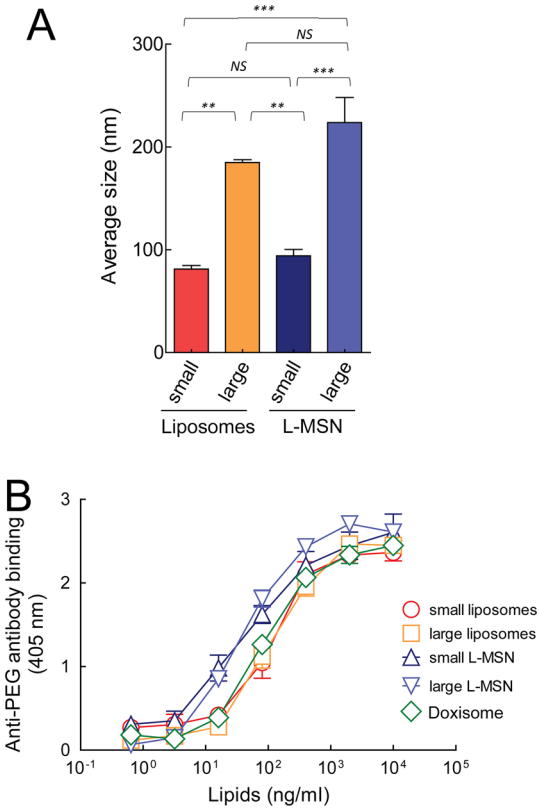

Figure 6. Characterization of size and PEG coating on NPs. (A) Mean diameter of NPs was calculated by dynamic light scattering (n = 3). Error bars, SD. Significant differences between mean values are shown; **$p \leq 0.01$; ***$p \leq 0.005$; NS, not significant. (B) Presence of PEG on NPs was determined by an anti-PEG sandwich ELISA. Error bars represent SD, n = 3.

3, 4, and 6 h) at 37 °C. The total lipid added to the cells was maintained constant at 5 μg/mL. The NPs remaining on the surface of the cells at each time point were removed by washing the cells with an acidic solution (Figure S4) as previously described[39] and then measuring the remaining fluorescence representing the internalized NPs. Here we used SKBR3 cells for all studies to eliminate confounding differences between cell types. Results were normalized to the fluorescence at time zero to account for differences in αPEG-H1 and αPEG-H2 receptor numbers. For example, 200% relative uptake means that the number of internalized NPs at that time exceeded by 2-fold the number of NPs that initially bound to the cells. The results show mean values from two independent experiments, each performed in triplicate. Endocytosis of small liposomes and small L-MSN into αPEG-H1/SKBR3 cells rapidly increased to a maximum of about 360 and 250% relative uptake, respectively, at 2 h but then decreased and became stable at about 200% relative uptake after 4–6 h incubation, suggesting recycling of some NPs out of the cells (Figure 7A). Consistent with our observations, HER1 receptors have been reported to possess a relatively low endocytic capacity, so that this pathway is easily saturated and can undergo a recycling process.[40−42] The large liposomes and large L-MSN were retained better than the small NPs, but their maximal uptake was significantly lower ($p \leq 0.005$) than the corresponding small NPs (239 ± 13% *versus* 359 ± 17% for large and small liposomes and 142 ± 7% *versus* 253 ± 15% for large and small L-MSN, respectively). In particular, the large L-MSN were taken up poorly *via* HER1-

DOI: 10.1021/acsnano.5b05661
ACS Nano 2016, 10, 648–662

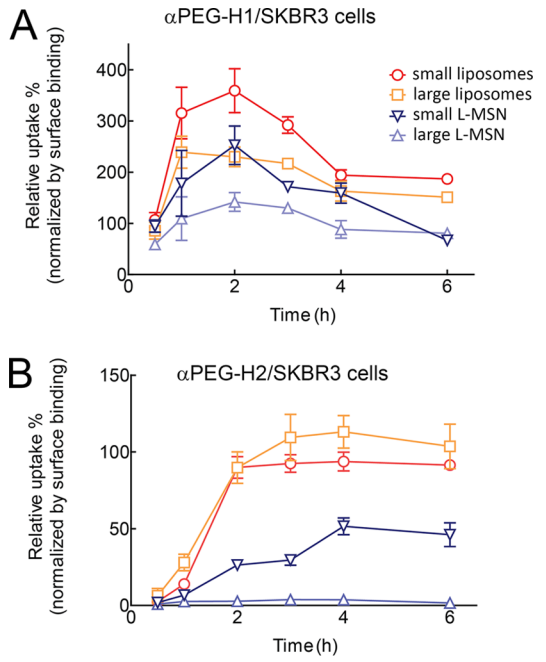

Figure 7. Cellular uptake of NPs depends on both NP properties and the targeted receptor. Fluorescent-labeled NPs were incubated with αPEG-H1/SKBR3 (A) or αPEG-H2/SKBR3 (B) cells at 37 °C for the indicated times before surface NPs were removed by an acid wash, and the remaining intracellular NPs were measured by FACS as described in the Methods section. The results are presented as the intracellular fluorescence at each time normalized to the initial surface fluorescence intensity at time zero. The experiment was repeated twice with three replicates each time, and the results show the mean values of all six replicates ± SD.

mediated endocytosis. In accord with our observations, the cellular uptake and exocytosis of transferrin-coated NPs, which also proceeds *via* a clathrin-dependent process, also depended on size with larger transferrin-coated gold NPs (100 nm), displaying about 2-fold slower exocytosis as compared to smaller transferrin-coated gold NPs (50 nm).[7,8] The mechanism for the differential size discrimination between HER1 endocytosis and recycling pathways remains to be determined but might be important for effective retention of targeted nanocargos in cancer cells.

Proteins can adsorb on NPs to form a "protein corona" that can alter cellular interactions and particle internalization. The degree of protein adsorption to NPs depends on many properties including the size, hardness, and degree of PEGylation.[43−45] We therefore measured the relative uptake of small and large liposomes and L-MSN into αPEG-H1/SKBR3 cells in culture medium with or without serum. We observed slightly greater internalization of all NPs in the presence of serum as compared to serum-free medium, although the difference was not statistically significant (Figure S5). These results suggest that protein adsorption to NPs did not significantly alter the internalization of the NPs *via* chimeric HER1 receptors on SKBR3 cells, consistent with previous studies demonstrating reduced protein adsorption to PEGylated NPs.[45]

HER2-mediated cellular uptake of PEGylated NPs in αPEG-H2/SKBR3 cells was substantially different than the uptake observed in αPEG-H1/SKBR3 cells. First, maximum uptake of NPs reached only about 120% relative uptake as compared to up to 360% in αPEG-H1/SKBR3 cells (Figure 7B). Second, both small and large flexible liposomes underwent endocytosis to similar degrees and with similar kinetics. Third, both small and large liposomes were well retained in the cells. Finally, the rigid L-MSN were poorly internalized with almost no uptake observed for the large L-MSN. Internalization of cargos by HER2 receptors is mediated by caveolae-dependent endocytosis.[46] The size of the caveolae-coated pits are ∼50 nm,[47] which may greatly hinder internalization of larger rigid NPs. Interestingly, large liposomes were internalized as well as small liposomes, suggesting that flexible NPs are preferred for effective uptake of targeted nanocargos *via* HER2. More flexible NPs may also display enhanced circulation and targeting compared to harder NPs *in vivo*.[48]

Comparison of HER1-Mediated Internalization by Chimeric Receptors and Antibody-Targeted NPs. We sought to further verify that SKBR3 cells engineered to express chimeric receptors could recapitulate internalization of antibody-targeted NPs by first covalently attaching anti-HER1 scFv to small and large liposomes and lipid-coated MSN. We then measured the intracellular uptake of the targeted NPs into SKBR3 cells using the identical protocol employed to measure the uptake of PEGylated NPs into αPEG-H1/SKBR3 cells. Comparison of the uptake of the targeted NPs into SKBR3 cells with the previously determined endocytosis of PEGylated NPs into αPEG-H1/SKBR3 cells (from Figure 7A) demonstrated qualitatively similar dependence on NP size and rigidity (Figure 8). For example, internalization of small αH1-IL and αH1-L-MSN into SKBR3 cells rapidly increased to a maximum of about 330 and 230% as compared to small liposomes (360%) and small L-MSN (250%) in αPEG-H1/SKBR3 cells (Figure 8A,C). Collectively, these results show that HER1 chimeric receptors can mimic the cellular uptake of anti-HER1 antibody-targeted NPs.

Effect of NP Size and Rigidity on Lysosomal Accumulation. We further examined the effect of NP properties on cellular routing to lysosomes. Colocalization of NPs and lysosomes was measured by incubating αPEG-H1/SKBR3 or αPEG-H2/SKBR3 cells with fluorescent-labeled PEGylated NPs for 2 h and then measuring the yellow colocalization of the fluorescence from the NPs (green) with the fluorescence of a lysosomal marker (red). The cellular location of the small or large liposomes and L-MSN was observed by confocal microscopy (Figure 9A). The relative intracellular uptake of the various NPs into αPEG-H1/SKBR3 cells after 2 h was similar to that previously observed (Figure 9B). Quantification of lysosomal colocalization showed that more than 50% of the small liposomes and small L-MSN were present in lysosomes after 2 h (Figure 9C). By contrast, accumulation of the large NPs in lysosomes was significantly lower (∼40%) at 2 h. These differences in lysosomal accumulation are unlikely due to differences in the rate of endocytosis since all NPs reached their maximum intracellular accumulation at about 2 h (Figure 7A).

The cellular routing of liposomes and L-MSN to lysosomes in αPEG-H2/SKBR3 cells was also observed by confocal microscopy (Figure 10A). The relative uptake of the different NPs into αPEG-H2/SKBR3 cells after 2 h was similar to previously determined values (Figure 10B). Relatively fewer small and large liposomes accumulated in lysosomes at 2 h as compared to the HER1 pathway (20% *vs* 45−60% of total NPs), but rigid L-MSN was more efficiently transported to lysosomes, especially the large L-MSN, which reached 51% accumulation in lysosomes (Figure 10C). Thus, more rigid NPs

DOI: 10.1021/acsnano.5b05661
ACS Nano 2016, 10, 648−662

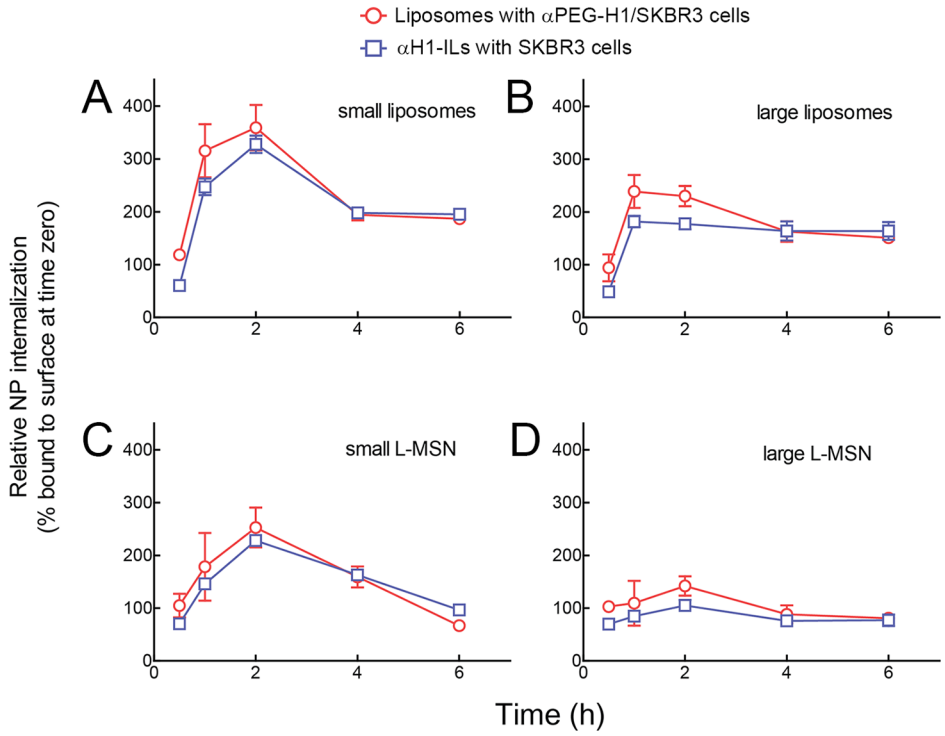

Figure 8. Comparison of cellular uptake of antibody-labeled NPs in SKBR3 cells and PEGylated NPs in αPEG-H1/SKBR3 cells. Fluorescent-labeled small αH1-liposomes (A), large αH1-liposomes (B), small αH1-L-MSN (C), and large αH1-L-MSN (D) were incubated with parental SKBR3 cells (blue squares) at 37 °C for the indicated times before surface NPs were removed by an acid wash, and the remaining intracellular NPs were measured by FACS as described in the Methods section. The results are presented as the intracellular fluorescence at each time normalized to the initial surface fluorescence intensity at time zero. The cellular uptake pattern was compared to PEGylated NPs taken up in SKBR3 cells that express chimeric HER1 receptors (red circles) at different times, as shown in Figure 7A. The results show the mean values of three replicates ± SD.

are taken up relatively poorly and are rapidly transported to lysosomes in αPEG-H2/SKBR3 cells, suggesting that hard NPs should not be used to deliver "delicate" nanocargos *via* the HER2 pathway.

Cellular Cytotoxicity of Doxisome Depends on the Route of Internalization. Our results indicate that flexible liposomes are more rapidly internalized by HER1 as compared by HER2. We therefore performed a simple experiment to determine whether targeting PEGylated liposomal doxorubicin (Doxisome) to αPEG-H1 or αPEG-H2 chimeric receptors would produce differential inhibition of SKBR3 breast cancer cell proliferation. SKBR3, αPEG-H1/SKBR3, and αPEG-H2/SKBR3 cells were incubated with different concentrations of Doxisome for 2 or 6 h. The cells were then washed, and cell proliferation was measured 2 days later. Doxisome significantly inhibited the proliferation of αPEG-H1/SKBR3 cells as compared to either SKBR3 or αPEG-H2/SKBR3 cells after both 2 h (Figure 11A) and 6 h (Figure 11B), consistent with greater uptake of liposomes *via* HER1. These results suggest that HER1 may be a good candidate to target liposomal doxorubicin for cancer therapy.

CONCLUSIONS

Ligand-targeted NPs are highly attractive for selective delivery of nanocargos to specific cellular targets. The therapeutic efficacy of targeted NPs depends on many factors including NP properties, targeting ligand, and cell type. Here we investigated a platform technology that may assist in the rational development of targeted stealth NPs. Chimeric receptors that can bind to PEG molecules on stealth NPs but mimic the function of HER1 or HER2 were expressed on cancer cells to mimic targeted NPs without the need to covalently attach targeting ligands to the NPs. Confocal imaging, FACS, and RNAi studies demonstrated that chimeric HER1 and HER2 receptors on cancer cells were predictive of the endocytosis and routing of ligand-targeted NP to endogenous HER1 and HER2 on target cells. Our study suggests that this approach can be extended to other receptor targets by fusing the αPEG antibody to the transmembrane/endodomain of specific receptors. One can envision that a panel of cells expressing different chimeric receptors could be developed to facilitate systematic screening for optimal cellular targets and NP properties for effective delivery and cellular response to nanocargos. It should also be possible to compare NP therapeutic activity in mice bearing tumors that express chimeric receptors as we previously demonstrated for tumors expressing a chimeric receptor based on the low-density lipoprotein receptor.[14] The major prerequisite for this approach is covalent attachment of PEG to the surface of the NPs, which is commonly used to improve the biological properties of many types of NPs including gold NPs, iron oxide NPs, PLGA NPs, mesoporous silica NPs, and liposomes.[49,50]

Cells expressing a chimeric receptor were used to investigate the influence of NP size and rigidity on endocytosis and lysosomal accumulation. In general, we observed more rapid internalization of NPs *via* HER1 as compared to HER2. Both large and small liposomes could be internalized *via* HER2, but rigid NPs were very poorly internalized by this pathway. Lysosomal accumulation of NPs targeted to HER1 depended primarily on size, whereas NP rigidity appeared to be the

DOI: 10.1021/acsnano.5b05661
ACS Nano 2016, 10, 648–662

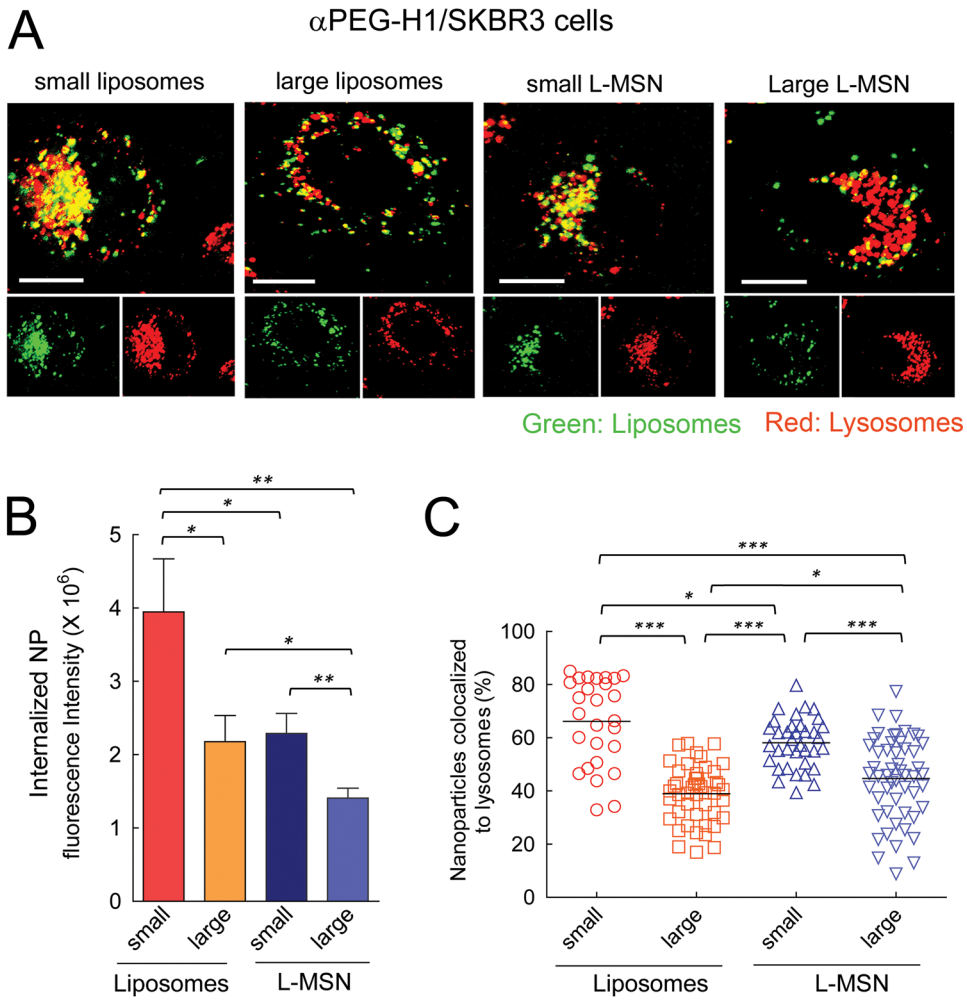

Figure 9. Lysosomal accumulation of stealth NPs in αPEG-H1/SKBR3 cells. (A) Lysosomes in αPEG-H1/SKBR3 cells were first labeled red with LysoTracker and then incubated for 2 h at 37 °C with fluorescent small liposomes, large liposomes, small L-MSN, or large L-MSN. Live cells were imaged on a confocal microscope. Scale bars = 10 μm. (B) Fluorescent intensity of internalized NPs was measured from confocal images. Results show mean values ± SD (n = 3); *$p \leq 0.05$; **$p \leq 0.01$. (C) Percentage of internalized NPs that colocalized with lysosomal markers was quantified from confocal images. The horizontal bars indicate mean values (n > 20). Significant differences between mean lysosomal colocalization are indicated: *$p \leq 0.05$; ***$p \leq 0.005$.

primary determinant of lysosomal accumulation for HER2. These studies emphasize the importance of optimizing NP properties for each specific cellular receptor target as well as for the desired intracellular routing of the nanocargo.

METHODS

Reagents. 1,2-Distearoyl-*sn*-glycero-3-phosphocholine (DSPC), 1,2-distearoyl-*sn*-glycero-3-phosphoethanolamine-*N*-[methoxy-(polyethylene glycol)-2000] (DSPE-PEG-2000), 1,2-distearoyl-*sn*-glycero-3-phosphoethanolamine-*N*-[maleimide (polyethylene glycol)-2000] (ammonium salt) (DSPE-PEG-Mal), and cholesterol were purchased from Avanti Polar Lipids, Inc. (Alabaster, AL). DiIC18(5) oil (1,1′-dioctadecyl-3,3,3′,3′-tetramethylindodicarbocyanine perchlorate) and large MSN (200 nm) were purchased from Life Technologies (Carlsbad, CA). Small MSNs (50 nm) were fabricated and purified as described.[51] G418, paraformaldehyde, and poly-L-lysine were from Sigma-Aldrich Corp. (St. Louis, MO). Competent *Escherichia coli* strains with AP2 shRNA-expressing pLKO_TRC005 (TRCN0000293892) and Eps15 shRNA pLKO.1 (TRCN0000007978) plasmids were obtained from the National RNAi Core Facility (Institute of Molecular Biology and Genomic Research Center, Academia Sinica).

Cell Lines. SKBR3 human breast adenocarcinoma cells (ATCC; HTB-30), A431 human epidermoid carcinoma cells (ATCC CRL-1555), and HT29 human colon carcinoma cells (ADCC HTB-38) were cultured in RPMI 1640 (Life Technologies) supplemented with 6 g/L HEPES, 2 g/L $NaHCO_3$, 10% heat-inactivated fetal bovine serum (HyClone), penicillin (100 units/mL), and streptomycin (100 μg/mL). GP2-293 cells (BD Biosciences, Franklin Lakes, NJ) and HEK-293 cells (CRL-1573, ATCC) were cultured in Dulbecco's modified Eagle's medium (DMEM) (Sigma-Aldrich) supplemented with 6 g/L HEPES, 3.7 g/L $NaHCO_3$, 10% heat-inactivated fetal bovine serum (HyClone, South Logan, Utah), penicillin (100 units/mL), and streptomycin (100 μg/mL). All cells were cultured at 37 °C in a humidified atmosphere of 5% CO_2 in air.

Construction and Transduction of αPEG-HER1 and αPEG-HER2 Chimeric Receptors. The vector pBABEpuro-ERBB2, containing the full-length human HER2 gene, was purchased from Addgene (plasmid # 40978; GenBank ID NM_004448.3). The full-length human HER1 gene was isolated from cultured A431 cells by reverse transcription using oligo dT primers. The HER1 gene was ligated into pCR-Blunt II-TOPO (Invitrogen) following the manufacturer's instructions. The positive clones were selected and confirmed by DNA sequencing. Truncated HER1 and HER2 genes encompassing the transmembrane and cytosolic domains (Supporting Information Table I) were amplified using *Taq* polymerase (Takara,

DOI: 10.1021/acsnano.5b05661
ACS Nano 2016, 10, 648–662

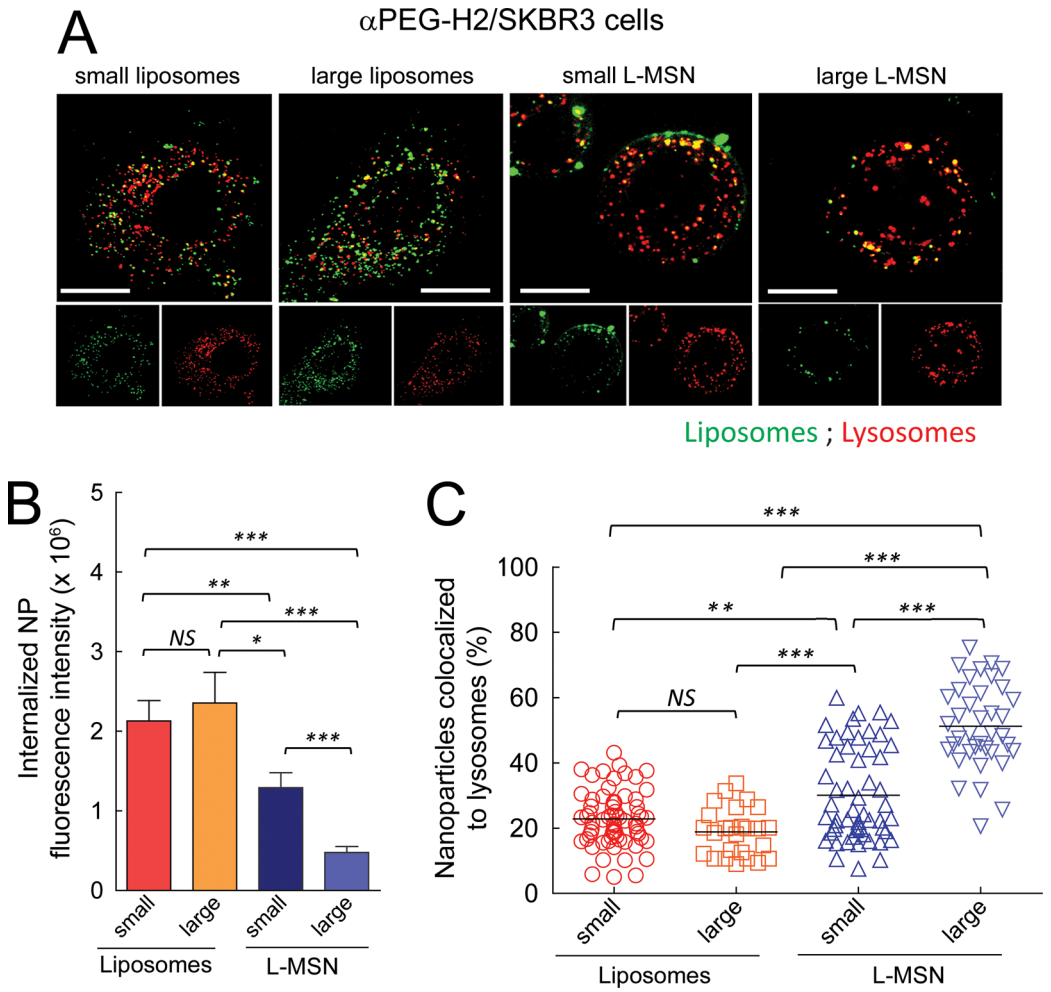

Figure 10. Lysosomal accumulation of NPs in αPEG-H2/SKBR3 cells. (A) Lysosomes in αPEG-H1/SKBR3 cells were labeled red with LysoTracker and then incubated for 2 h at 37 °C with fluorescent small liposomes, large liposomes, small L-MSN, or large L-MSN. Live cells were imaged on a confocal microscope. Scale bars = 10 μm. (B) Fluorescent intensity of internalized NPs was measured from confocal images. Results show mean values ± SD (n = 3); *$p \leq 0.05$; **$p \leq 0.01$; ***$p \leq 0.005$; NS, not significant. (C) Percentage of internalized NPs that colocalized with lysosomal markers was quantified from confocal images. The horizontal bars indicate mean values (n > 20). Significant differences between mean lysosomal colocalization are indicated: **$p \leq 0.01$; ***$p \leq 0.005$; NS, not significant.

Shiga, Japan) using a 5′-primer containing a *Sal*I site and a 3′-primer containing a Cla I site (Supporting Information Table II). The PCR products were digested with *Sal*I and Cla I and then inserted into the retroviral expression vector pLNCX-αPEG[14] in frame with the 3′ end of the gene coding an αPEG Fab fragment derived from the AGP3 anti-PEG monoclonal antibody,[52] to generate pLNCX-αPEG-HER1 and pLNCX-αPEG-HER2 plasmids. Both chimeric receptors have an HA epitope tag present at their N-terminus for immunodetection of the receptors.

Recombinant retroviral particles were produced by cotransfection of the pMD.G VSV-G envelope plasmid (Clontech Laboratories Inc., Palo Alto, CA) with pLNCX-αPEG-HER1 or pLNCX-αPEG-HER2 into GP2-293 cells. After 48 h, the culture medium was filtered, mixed with 8 μg/mL Polybrene (Sigma-Aldrich), and added to SKBR3 or HT29 cells. The cells were selected in complete medium supplemented with 0.5 mg/mL G418 (Calbiochem, San Diego, CA, USA) followed by fluorescence-activated cell sorting to generate αPEG-H1/HT29 cells that express anti-PEG-HER1 chimeric receptors in HT29 colon cancer cells or αPEG-H1/SKBR3 or αPEG-H2/SKBR3 cells which express anti-PEG-HER1 or anti-PEG-HER2 chimeric receptors in SKBR3 cells, respectively.

Expression Levels of Chimeric Receptors on Cancer Cells. The expression of chimeric receptors on stably transfected HT29 and SKBR3 cells was determined by incubating 5 × 10^5 αPEG-H1/HT29, αPEG-H1/SKBR3, αPEG-H2/SKBR3, HT29, and SKBR3 cells with 1 μg/mL mouse anti-HA antibody in cold 0.05% bovine serum albumin (BSA)/PBS for 1 h on ice to detect the HA epitope tag present at the N-terminus of the chimeric receptors. After being washed with cold 0.05% BSA/PBS three times, the cells were incubated with 1 μg/mL FITC-conjugated goat anti-mouse IgG (Fc) (Jackson ImmunoResearch Laboratories) for 1 h on ice. The cells were washed with cold 0.05% BSA/PBS three times before the cells were stained with propidium iodide (Invitrogen) to identify dead cells. The surface fluorescence of FITC on 10^4 viable cells was measured on a LSR II flow cytometer (BD Biosciences, Mountain View, CA, USA).

Construction of scFv against HER1 and HER2. A single-chain antibody (scFv) against human HER1 was generated based on the 11F8 DNA[53,54] sequence by assembly PCR. A scFv against human HER2 was cloned from the pBub-YCMC plasmid kindly provided by Prof. Louis M. Weiner of Fox Chase Cancer Center, Philadelphia.[55] The αHER1 and aHER2 scFv were cloned into the retroviral vector pLNCX (BD Biosciences) with a signal sequence at the N-terminus of the scFv to direct their secretion from mammalian cells.[54,56] A 6× histidine (His) tag and a cysteine residue were fused to the C-terminus of the scFv for purification and site-specific attachment to liposomes. The final retroviral expression vectors were named pLNCX-αHER1-His-C and pLNCX-αHER2-His-C, respectively.

Production and Purification of scFv Antibodies. Recombinant retroviral particles were produced by cotransfection of pMD.G, VSV-G envelope plasmid (RNAi core, Academia Sinica, Taipei, Taiwan) with

DOI: 10.1021/acsnano.5b05661
ACS Nano 2016, 10, 648–662

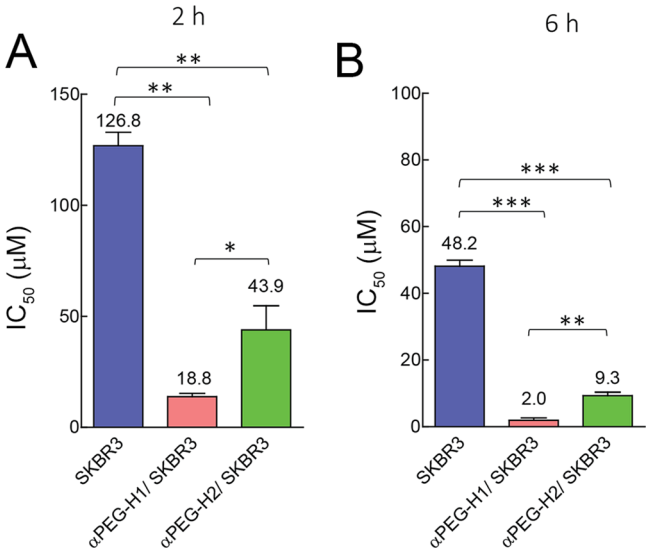

Figure 11. Inhibition of cancer cell proliferation by Doxisome. SKBR3, αPEG-H1/SKBR3, and αPEG-H2/SKBR3 cells were incubated with serial dilutions of Doxisome in triplicate for 2 or 6 h before fresh medium was added for 2 days, and then cellular proliferation was measured by a ^{3}H-thymidine incorporation assay. The concentration of Doxisome causing 50% inhibition (IC_{50}) of SKBR3, αPEG-H1/SKBR3, and αPEG-H2/SKBR3 cells after 2 h (A) and 6 h (B) is shown. Mean ± SD; $n = 3$. Significant differences in IC_{50} values are indicated: *$p \leq 0.05$; **$p \leq 0.01$; ***$p \leq 0.005$.

pLNCX-αHER1-His-C or pLNCX-αHER2-His-C into GP2-293 cells. After 48 h, the culture medium was filtered, mixed with 8 μg/mL Polybrene, and added to HEK-293 cells. The cells were selected in complete medium supplemented with 0.5 mg/mL G418 to generate stable producer cells that secrete αHER1 or αHER2 scFv.

The cell culture medium of stable HEK-293 producer cells grown in DMEM medium was harvested, and the cells were removed by filtration through a 0.45 μm filter. scFv were purified as described.[57] Briefly, scFv were precipitated and washed once with 60% saturated ammonium sulfate solution. The pellet was dissolved in binding buffer (0.5 M NaCl, 20 mM Tris/HCl, pH 7.4) and purified on a Co^{2+} TALON Superflow column (GE Healthcare). The scFv were dialyzed three times against PBS at 4 °C, concentrated on a 30 kDa cutoff Amicon Ultra (Millipore, Billerica, MA), and sterile filtered. scFv concentrations were determined with the bicinchoninic acid (BCA) protein kit (Thermo Scientific).

Preparation of Immunoliposomes. Liposomes containing Mal-PEG_{2000}-DSPE were prepared by dissolving DSPC, PEG_{2000}-DSPE, Mal-PEG_{2000}-DSPE, cholesterol, and DiIC18(5) in chloroform at a 64.5:4:1:30:0.5 molar ratio. A dried lipid film was formed at 65 °C by rotary evaporation (Büchi, Rotavapor RII, Switzerland) and rehydrated in Tris-buffered saline (TBS; 50 mM Tris-HCl, 150 mM NaCl, pH 7.4; degassed with sonication plus vacuum) at 65 °C to a final lipid concentration of 5 mg/mL. The liposomal suspension was submitted to five freeze/thaw cycles using liquid nitrogen and a water bath followed by extrusion 21 times at 70 °C through 400, 200, and 80 nm polycarbonate membranes using a mini-extruder (Avanti Polar Lipids). The αHER1 or αHER2 scFv were reduced for 30 min at 37 °C with 5 mM dithiothreitol, and reducing agent was then removed by gel filtration on a Sephadex G-25 column. The reduced αHER1 or αHER2 scFv fragments were combined with liposomes at a molar ratio of 5:1 (scFv: Mal-PEG_{2000}-DSPE) overnight at 4 °C with shaking under a N_2 atmosphere.[58] Unconjugated scFv were removed by centrifugation at 40 000 rpm for 40 min at 4 °C. The resulting immunoliposomes with covalently attached αHER1 or αHER2 scFv are denoted as αH1-IL or αH2-IL, respectively.

Preparation of PEGylated Liposomes. PEG-liposomes were made in an analogous fashion as the immunoliposomes except that DSPC, PEG_{2000}-DSPE, cholesterol, and DiIC18(5) were dissolved in chloroform at a 64.5:5:30:0.5 molar ratio, respectively. Large and small PEG-liposomes were made by extrusion 21 times at 70 °C through 400 and 200 nm polycarbonate membranes, whereas small PEG-liposomes were made by extrusion 21 times at 70 °C through 400, 200, 80, and 50 nm polycarbonate membranes. In all cases, the final lipid concentration of liposomes was measured by Bartlett's assay.[59] Liposomal particle size was determined by dynamic light scattering on a Zetasizer nano ZS (Malvern Instrument Ltd., UK).

Preparation of PEGylated Lipid-Coated MSNs. For generation of PEGylated lipid-coated MSN, DSPC, DSPE-PEG_{2000}, cholesterol, and DiIC18(5) were dissolved in chloroform at a 64.5:5:30:0.5 molar ratio, respectively. A dried lipid film was formed at 65 °C by rotary evaporation and rehydrated in TBS at 65 °C to a final lipid concentration of 20 mg/mL. Large MSN (~200 nm) and small MSN (~80 nm) were washed twice with 70% EtOH and rehydrated in TBS at 10 mg/mL followed by sonication for 10 min. The lipids were added drop by drop to MSN with vortexing, and the mixture was submitted to 11 freeze/thaw cycles, followed by extrusion 21 times at 70 °C through 400 and 200 nm polycarbonate membranes to generate large lipid-coated MSN (L-MSN) or by extrusion 21 times at 70 °C through 400, 200, and 80 nm polycarbonate membranes to generate small L-MSN. Free lipids were removed by centrifugation (2300*g*, 5 min) and washing with PBS three times.

Comparison of Liposome and Immunoliposome Binding to Cells. The binding of PEG-liposomes to cells was measured by incubating 5 × 10^5 αPEG-H1/HT29, αPEG-H1/SKBR3, αPEG-H2/SKBR3, HT29, or SKBR3 cells with 5 μg/mL PEGylated liposomes labeled with DiIC18(5) in cold 0.05% BSA/PBS for 1 h on ice. The binding of immunoliposomes to cancer cells was determined by incubating 5 × 10^5 SKBR3 (HER1$^+$ and HER2$^+$) or HT29 (HER1$^+$) cells with 10 μg/mL αH1-IL or αH2-IL on ice for 1 h. After being washed with cold 0.05% BSA/PBS three times, the cells were stained with propidium iodide viability dye, and the surface fluorescence of liposomes on 10^4 viable cells was measured on a LSR II flow cytometer (BD Biosciences, Mountain View, CA, USA). Results are presented as mean fluorescence intensities (MFI).

siRNA Transfection. Small hairpin RNA (shRNA) plasmids for the AP2 and Eps15 genes were obtained from the National RNAi Core Facility (Academia Sinica, Taipei, Taiwan). For AP2 or Eps15 knockdown, αPEG-H1/HT29, αPEG-H2/SKBR3, HT29, and SKBR3 cells were seeded overnight in 6-well plates at a density of 1 × 10^5 cells per well. Fresh medium without serum or antibiotics containing 8 μg/mL Polybrene (Sigma-Aldrich) and 10 μg/mL of lentivirus carrying shRNA targeting AP2 or Eps15 was added to the cells for 24 h. After lentiviral infection, the cells were selected in 2 μg/mL puromycin for 2 days.

Confocal Imaging of Liposomes in Cancer Cells. Cells (2 × 10^5) in RPMI medium supplemented with 10% FBS (RMPI/10) were seeded on a glass slide precoated with 40 μg/mL poly-L-lysine overnight. The cells were incubated with 0.1 μg/mL LysoTracker Red DND99 (Sigma-Aldrich) to stain lysosomes or 1 μg/mL Hoechst 33342 (Invitrogen) to stain nuclei in RPMI for 30 min at 37 °C in a humidified atmosphere of air containing 5% CO_2. After being washed with RPMI/10, cells were incubated with 10 μg/mL DiIC18(5)-labeled PEGylated liposomes, immunoliposomes, or L-MSN for 2 h at 37 °C before the fluorescence signals were detected on a Zeiss LSM780 laser scanning microscope (Carl Zeiss AG, Germany). Initial digital image processing was performed using Zeiss LSM browser at excitation and emission wavelengths of 560 and 580 nm for LysoTracker Red DND99 and 650 and 675 nm for DiIC18(5). Colocalization studies were performed using ImageJ (NIH) by computing the overlap of individual pixels from the NP and lysosome fluorescence channels. Single cells were gated in each image, and the overlap coefficient m_1 was calculated according to Manders to determine the true degree of colocalization.[60] $S1$ represents signal intensity of pixels in the NP channel, and $S1_{i,coloc}$ represents the overlap of NP pixels and lysosome pixels. For example, if the green–red pair of channels is selected, and $m_1 = 0.23$; this means that 23% of green pixels colocalize with red pixels.

DOI: 10.1021/acsnano.5b05661
ACS Nano 2016, 10, 648–662

$$m_1 = \frac{\sum_i SI_{i,\mathrm{coloc}}}{\sum_i SI_i}$$

Detection of PEG on PEGylated NPs Using Sandwich ELISA. Maxisorp flat-bottom 96-well plates were coated with 50 μL/well of AGP4 anti-PEG antibody[38] (20 μg/mL) in coating buffer (100 mM Na_2CO_3, pH 8.0) at room temperature and then at 4 °C overnight. The wells were emptied and blocked with 5% skim milk in PBS at 37 °C for 2 h and then washed twice in PBS. PEGylated NPs or Doxisome (PEGylated liposomal doxorubicin; Taiwan Liposome Company, Ltd.) were serially diluted in dilution buffer (2% skim milk in PBS), added to wells (50 μL/well), and incubated at room temperature for 2 h. After being washed with PBS three times, the wells were sequentially incubated with 50 μL/well of biotinylated anti-PEG antibody (3.3-biotin, 5 μg/mL in dilution buffer) and 50 μL/well horseradish peroxidase-conjugated streptavidin (1 μg/mL in dilution buffer) (Jackson ImmunoResearch, West Grove, PA).[38] After being incubated for 1 h at RT, the plates were washed with PBS eight times. The bound peroxidase activity was measured by adding 100 μL/well ABTS solution [0.4 mg/mL, 2,2′-azinobis(3-ethylbenzthiazoline-6-sulfonic acid), 0.003% H_2O_2, and 100 mM phosphate-citrate, pH 4.0) at room temperature. The absorbance (405 nm) of the wells was measured in a microplate reader (Molecular Device, Sunnyvale, CA).

Cellular Uptake of NPs Measured by FACs. To compare the cellular uptake of different PEGylated NPs by cells expressing chimeric HER1 or HER2 receptors, 5×10^5 αPEG-H1/HT29, αPEG-H1/SKBR3, αPEG-H2/SKBR3, HT29, or SKBR3 cells were incubated with different DiIC18(5)-labeled NPs at equal concentrations of lipids (5 μg/mL) in RPMI medium for 0.5, 1, 2, 3, 4, and 6 h at 37 °C. The unbound NPs were removed by washing the cells twice with 0.05% BSA/PBS, followed by treatment of the cells with cold citric acid buffer (pH 3.0) for 3 min (acid wash)[39] to remove the noninternalized NPs before washing again with 0.05% BSA/PBS twice. The cells were stained with propidium iodide viability dye, and the fluorescence of the NPs in 10^4 viable cells was measured on a LSR II flow cytometer (BD Biosciences, Mountain View, CA, USA).

To measure the initial binding of NPs to the cells, 5×10^5 cells were incubated with the different NPs at equal concentrations of lipids (5 μg/mL) in RPMI medium for 1 h on ice. After being washed with cold 0.05% BSA/PBS three times, the cells were stained with propidium iodide, and the surface fluorescence of liposomes on 10^4 viable cells was measured on a LSR II flow cytometer (BD Biosciences, Mountain View, CA, USA). The relative uptake (%) was corrected by subtracting NP background binding to cells and then normalized to the amount of NPs binding to the cells at time zero by the formula:

$$\begin{aligned}\text{relative uptake \%} = [&(\text{NP MFI at each time after acid wash} \\ &- \text{initial NP MFI after acid wash}) \\ &/(\text{initial NP MFI at 4 °C})] \times 100\end{aligned}$$

where NP MFI is the NP mean fluorescence intensity.

Cell Proliferation Assay. SKBR3, αPEG-H1/SKBR3, and αPEG-H2/SKBR3 cells (1×10^4) were seeded in 96-well plates overnight. The next day, graded concentrations of Doxisome were added in triplicate to the wells for 2 or 6 h at 37 °C. After the medium was removed and fresh medium was added, the cells were incubated for 48 h to allow the drug to act on the cells. The cells were then pulsed with ^{3}H-thymidine (1 μCi/well) for 18 h to measure the rate of DNA synthesis, which reflects the total cell proliferative capacity in each well. The cells were harvested, and the radioactivity was measured on a TopCount microplate scintillation counter (Packard, Detroit, MI). Results are expressed as percent ^{3}H-thymidine incorporation compared with untreated control cells by the following formula:

$$^3\text{H-thymidine incorporation (\%)} = \frac{\text{sample cpm}}{\text{untreated control cpm}} \times 100$$

IC_{50} values were calculated by fitting the data to a log (inhibitor) *versus* response (variable slopes model) with Prism 5 software (Graphpad Software, San Diego, CA).

Statistical Analysis. Statistical significance of differences between mean values was estimated with Graphpad or Excel (Microsoft, Redmond, WA) using the independent Student's *t* test for unequal variances; *p* values <0.05 were considered to be statistically significant.

ASSOCIATED CONTENT

Supporting Information

The Supporting Information is available free of charge on the ACS Publications website at DOI: 10.1021/acsnano.5b05661.

Supplemental methods, retention of fluorescent dye in NPs (Figure S1), binding of anti-HER1 and anti-HER2 scFv to cancer cells (Figure S2), effect of PEG density on liposome internalization (Figure S3), removal of surface-bound NPs by acid wash (Figure S4), and effect of serum proteins on liposome internalization (Figure S5) (PDF)

AUTHOR INFORMATION

Corresponding Authors

*E-mail: sroff@ibms.sinica.edu.tw.

*E-mail: tlcheng@kmu.edu.tw.

Author Contributions

¶W.-C.H. and P.-A.B. contributed equally to this work.

Notes

The authors declare no competing financial interest.

ACKNOWLEDGMENTS

This work was supported by a grant from the Academia Sinica Research Program on Nanoscience and Nanotechnology. We thank Ms. Chia-Chen Tai and Ms. Tzu-Wen Tai of the Flow Cytometry Core, Scientific Instrument Center at the Institute of Biomedical Sciences, Academia Sinica, Taipei, Taiwan, for assistance with the LSR II flow cytometer. In addition, we thank the Protein Mass Core, Scientific Instrument Center at the Institute of Biomedical Sciences, Academia Sinica, Taipei, Taiwan, for antibody molecular weight measurements. The National RNAi Core Facility (Institute of Molecular Biology/Genomic Research Center, Academia Sinica, Taipei, Taiwan) is gratefully acknowledged for help with providing RNAi lentiviruses. We also thank the staff at the DNA sequencing core facility and the confocal microscopy core facility of the Institute of Biomedical Sciences for their technical assistance.

REFERENCES

(1) Torchilin, V. Tumor Delivery of Macromolecular Drugs Based on the Epr Effect. *Adv. Drug Delivery Rev.* **2011**, *63*, 131−135.

(2) Denholt, C. L.; Hansen, P. R.; Pedersen, N.; Poulsen, H. S.; Gillings, N.; Kjaer, A. Identification of Novel Peptide Ligands for the Cancer-Specific Receptor Mutation EFGRvIII Using a Mixture-Based Synthetic Combinatorial Library. *Biopolymers* **2009**, *91*, 201−206.

(3) Torchilin, V. P. Multifunctional Nanocarriers. *Adv. Drug Delivery Rev.* **2012**, *64*, 302−315.

(4) Wang, A. Z.; Langer, R.; Farokhzad, O. C. Nanoparticle Delivery of Cancer Drugs. *Annu. Rev. Med.* **2012**, *63*, 185−198.

(5) Steichen, S. D.; Caldorera-Moore, M.; Peppas, N. A. A Review of Current Nanoparticle and Targeting Moieties for the Delivery of Cancer Therapeutics. *Eur. J. Pharm. Sci.* **2013**, *48*, 416−427.

(6) Cui, C.; Xue, Y. N.; Wu, M.; Zhang, Y.; Yu, P.; Liu, L.; Zhuo, R. X.; Huang, S. W. Cellular Uptake, Intracellular Trafficking, and Antitumor Efficacy of Doxorubicin-Loaded Reduction-Sensitive Micelles. *Biomaterials* **2013**, *34*, 3858−3869.

DOI: 10.1021/acsnano.5b05661
ACS Nano 2016, 10, 648−662

(7) Chithrani, B. D.; Ghazani, A. A.; Chan, W. C. Determining the Size and Shape Dependence of Gold Nanoparticle Uptake into Mammalian Cells. *Nano Lett.* **2006**, *6*, 662−668.
(8) Chithrani, B. D.; Chan, W. C. Elucidating the Mechanism of Cellular Uptake and Removal of Protein-Coated Gold Nanoparticles of Different Sizes and Shapes. *Nano Lett.* **2007**, *7*, 1542−1550.
(9) Jiang, W.; Kim, B. Y. S.; Rutka, J. T.; Chan, W. C. W. Nanoparticle-Mediated Cellular Response Is Size-Dependent. *Nat. Nanotechnol.* **2008**, *3*, 145−150.
(10) Nativo, P.; Prior, I. A.; Brust, M. Uptake and Intracellular Fate of Surface-Modified Gold Nanoparticles. *ACS Nano* **2008**, *2*, 1639−1644.
(11) Barua, S.; Yoo, J. W.; Kolhar, P.; Wakankar, A.; Gokarn, Y. R.; Mitragotri, S. Particle Shape Enhances Specificity of Antibody-Displaying Nanoparticles. *Proc. Natl. Acad. Sci. U. S. A.* **2013**, *110*, 3270−3275.
(12) Li, M. H.; Choi, S. K.; Leroueil, P. R.; Baker, J. R., Jr. Evaluating Binding Avidities of Populations of Heterogeneous Multivalent Ligand-Functionalized Nanoparticles. *ACS Nano* **2014**, *8*, 5600−5609.
(13) Hong, S.; Leroueil, P. R.; Majoros, I. J.; Orr, B. G.; Baker, J. R.; Banaszak Holl, M. M. The Binding Avidity of a Nanoparticle-Based Multivalent Targeted Drug Delivery Platform. *Chem. Biol.* **2007**, *14*, 107−115.
(14) Chuang, K. H.; Wang, H. E.; Chen, F. M.; Tzou, S. C.; Cheng, C. M.; Chang, Y. C.; Tseng, W. L.; Shiea, J.; Lin, S. R.; Wang, J. Y.; Chen, B. M.; Roffler, S. R.; Cheng, T. L. Endocytosis of Pegylated Agents Enhances Cancer Imaging and Anticancer Efficacy. *Mol. Cancer Ther.* **2010**, *9*, 1903−1912.
(15) O'Brien, M. E. R.; Wigler, N.; Inbar, M.; Rosso, R.; Grischke, E.; Santoro, A.; Catane, R.; Kieback, D. G.; Tomczak, P.; Ackland, S. P.; Orlandi, F.; Mellars, L.; Alland, L.; Tendler, C. Reduced Cardiotoxicity and Comparable Efficacy in a Phase III Trial of Pegylated Liposomal Doxorubicin HCl (Caelyx (Tm)/Doxil (R)) *Versus* Conventional Doxorubicin for First-Line Treatment of Metastatic Breast Cancer. *Ann. Oncol.* **2004**, *15*, 440−449.
(16) Kim, D. W.; Kim, S. Y.; Kim, H. K.; Kim, S. W.; Shin, S. W.; Kim, J. S.; Park, K.; Lee, M. Y.; Heo, D. S. Multicenter Phase II Trial of Genexol-PM, a Novel Cremophor-Free, Polymeric Micelle Formulation of Paclitaxel, with Cisplatin in Patients with Advanced Non-Small-Cell Lung Cancer. *Ann. Oncol.* **2007**, *18*, 2009−2014.
(17) Kim, H. J.; Kim, K. H.; Yun, J.; Kim, S. H.; Kim, H. J.; Lee, S. C.; Bae, S. B.; Kim, C. K.; Lee, N. S.; Lee, K. T.; Kim, D. J.; Park, S. K.; Won, J. H.; Hong, D. S.; Park, H. S. Phase Ii Clinical Trial of Genexol (R) (Paclitaxel) and Carboplatin for Patients with Advanced Non-Small Cell Lung Cancer. *Cancer Res. Treat.* **2011**, *43*, 19−23.
(18) Martinelli, E.; De Palma, R.; Orditura, M.; De Vita, F.; Ciardiello, F. Anti-Epidermal Growth Factor Receptor Monoclonal Antibodies in Cancer Therapy. *Clin. Exp. Immunol.* **2009**, *158*, 1−9.
(19) Parker, P. J.; Young, S.; Gullick, W. J.; Mayes, E. L. V.; Bennett, P.; Waterfield, M. D. Monoclonal-Antibodies against the Human Epidermal Growth-Factor Receptor from A431 Cells - Isolation, Characterization, and Use in the Purification of Active Epidermal Growth-Factor Receptor. *J. Biol. Chem.* **1984**, *259*, 9906−9912.
(20) Baselga, J.; Albanell, J. Mechanism of Action of Anti-HER2Monoclonal Antibodies. *Ann. Oncol.* **2001**, *12*, 35−41.
(21) Emde, A.; Kostler, W. J.; Yarden, Y. Association of, R.; Oncology of the Mediterranean, a., Therapeutic Strategies and Mechanisms of Tumorigenesis of HER2-Overexpressing Breast Cancer. *Crit. Rev. Oncol. Hematol.* **2012**, *84*, e49−e57.
(22) Baselga, J. The EGFR as a Target for Anticancer Therapy - Focus on Cetuximab. *Eur. J. Cancer* **2001**, *37*, S16−S22.
(23) Messersmith, W. A.; Hidalgo, M. Panitumumab, a Monoclonal Anti-Epidermal Growth Factor Receptor Antibody in Colorectal Cancer: Another One or the One? *Clin. Cancer Res.* **2007**, *13*, 4664−4666.
(24) Hurvitz, S. A.; Shatsky, R.; Harbeck, N. Afatinib in the Treatment of Breast Cancer. *Expert Opin. Invest. Drugs* **2014**, *23*, 1039−1047.
(25) Gajria, D.; Chandarlapaty, S. HER2-Amplified Breast Cancer: Mechanisms of Trastuzumab Resistance and Novel Targeted Therapies. *Expert Rev. Anticancer Ther.* **2011**, *11*, 263−275.
(26) Munster, P. N.; Miller, K.; Krop, I. E.; Dhindsa, N.; Reynolds, J.; Geretti, E.; Niyikiza, C.; Nielsen, U.; Hendriks, B.; Wickham, T. J.; Moyo, V. M.; LoRusso, P. A Phase I Study of MM-302, a HER2-Targeted Liposomal Doxorubicin, in Patients with Advanced, HER2-Positive (HER2+) Breast Cancer. *J. Clin. Oncol.* **2012**, *30*, 1−5.
(27) Mamot, C.; Ritschard, R.; Wicki, A.; Stehle, G.; Dieterle, T.; Bubendorf, L.; Hilker, C.; Deuster, S.; Herrmann, R.; Rochlitz, C. Tolerability, Safety, Pharmacokinetics, and Efficacy of Doxorubicin-Loaded Anti-EGFR Immunoliposomes in Advanced Solid Tumours: A Phase 1 Dose-Escalation Study. *Lancet Oncol.* **2012**, *13*, 1234−1241.
(28) Diermeier-Daucher, S.; Breindl, S.; Buchholz, S.; Ortmann, O.; Brockhoff, G. Modular Anti-EGFR and Anti-HER2 Targeting of SK-BR-3 and BT474 Breast Cancer Cell Lines in the Presence of ErbB Receptor-Specific Growth Factors. *Cytometry, Part A* **2011**, *79A*, 684−693.
(29) Woodburn, J. R. The Epidermal Growth Factor Receptor and Its Inhibition in Cancer Therapy. *Pharmacol. Ther.* **1999**, *82*, 241−250.
(30) Rappoport, J. Z.; Simon, S. M. Endocytic Trafficking of Activated EGFR Is AP-2 Dependent and Occurs through Preformed Clathrin Spots. *J. Cell Sci.* **2009**, *122*, 1301−1305.
(31) Husnjak, K.; Dikic, I. EGFR Trafficking: Parkin' in a Jam. *Nat. Cell Biol.* **2006**, *8*, 787−788.
(32) Robinson, M. S. Adaptins. *Trends Cell Biol.* **1992**, *2*, 293−297.
(33) Robinson, M. S. The Role of Clathrin, Adapters and Dynamin in Endocytosis. *Curr. Opin. Cell Biol.* **1994**, *6*, 538−544.
(34) Roxrud, I.; Raiborg, C.; Pedersen, N. M.; Stang, E.; Stenmark, H. An Endosomally Localized Isoform of Eps15 Interacts with Hrs to Mediate Degradation of Epidermal Growth Factor Receptor. *J. Cell Biol.* **2008**, *180*, 1205−1218.
(35) Saha, A.; Basiruddin, S. K.; Maity, A. R.; Jana, N. R. Synthesis of Nanobioconjugates with a Controlled Average Number of Biomolecules between 1 and 100 Per Nanoparticle and Observation of Multivalency Dependent Interaction with Proteins and Cells. *Langmuir* **2013**, *29*, 13917−13924.
(36) Elias, D. R.; Poloukhtine, A.; Popik, V.; Tsourkas, A. Effect of Ligand Density, Receptor Density, and Nanoparticle Size on Cell Targeting. *Nanomedicine* **2013**, *9*, 194−201.
(37) Owen, S. C.; Patel, N.; Logie, J.; Pan, G. H.; Persson, H.; Moffat, J.; Sidhu, S. S.; Shoichet, M. S. Targeting HER2+ Breast Cancer Cells: Lysosomal Accumulation of Anti-HER2 Antibodies Is Influenced by Antibody Binding Site and Conjugation to Polymeric Nanoparticles. *J. Controlled Release* **2013**, *172*, 395−404.
(38) Su, Y. C.; Chen, B. M.; Chuang, K. H.; Cheng, T. L.; Roffler, S. R. Sensitive Quantification of Pegylated Compounds by Second-Generation Anti-Poly(Ethylene Glycol) Monoclonal Antibodies. *Bioconjugate Chem.* **2010**, *21*, 1264−1270.
(39) Kessner, S.; Krause, A.; Rothe, U.; Bendas, G. Investigation of the Cellular Uptake of E-Selectin-Targeted Immunoliposomes by Activated Human Endothelial Cells. *Biochim. Biophys. Acta, Biomembr.* **2001**, *1514*, 177−190.
(40) Wiley, H. S. Anomalous Binding of Epidermal Growth Factor to A431 Cells Is Due to the Effect of High Receptor Densities and a Saturable Endocytic System. *J. Cell Biol.* **1988**, *107*, 801−810.
(41) Hoffmann, T.; Hafner, D.; Ballo, H.; Haas, I.; Bier, H. Antitumor Activity of Anti-Epidermal Growth Factor Receptor Monoclonal Antibodies and Cisplatin in Ten Human Head and Neck Squamous Cell Carcinoma Lines. *Anticancer Res.* **1997**, *17*, 4419−4425.
(42) Oh, N.; Park, J.-H. Endocytosis and Exocytosis of Nanoparticles in Mammalian Cells. *Int. J. Nanomed.* **2014**, *9*, 51.
(43) Lundqvist, M.; Stigler, J.; Elia, G.; Lynch, I.; Cedervall, T.; Dawson, K. A. Nanoparticle Size and Surface Properties Determine the Protein Corona with Possible Implications for Biological Impacts. *Proc. Natl. Acad. Sci. U. S. A.* **2008**, *105*, 14265−14270.

DOI: 10.1021/acsnano.5b05661
ACS Nano 2016, 10, 648−662

(44) Casals, E.; Pfaller, T.; Duschl, A.; Oostingh, G. J.; Puntes, V. Time Evolution of the Nanoparticle Protein Corona. *ACS Nano* **2010**, *4*, 3623−3632.
(45) Walkey, C. D.; Olsen, J. B.; Guo, H.; Emili, A.; Chan, W. C. W. Nanoparticle Size and Surface Chemistry Determine Serum Protein Adsorption and Macrophage Uptake. *J. Am. Chem. Soc.* **2012**, *134*, 2139−2147.
(46) Sekhar, S. C.; Kasai, T.; Satoh, A.; Shigehiro, T.; Mizutani, A.; Murakami, H.; El-Aarag, B. Y. A.; Salomon, D. S.; Massaguer, A.; de Llorens, R.; Seno, M. Identification of Caveolin-1 as a Potential Causative Factor in the Generation of Trastuzumab Resistance in Breast Cancer Cells. *J. Cancer* **2013**, *4*, 391−401.
(47) Gilbert, A.; Paccaud, J. P.; Foti, M.; Porcheron, G.; Balz, J.; Carpentier, J. L. Direct Demonstration of the Endocytic Function of Caveolae by a Cell-Free Assay. *J. Cell Sci.* **1999**, *112*, 1101−1110.
(48) Anselmo, A. C.; Zhang, M.; Kumar, S.; Vogus, D. R.; Menegatti, S.; Helgeson, M. E.; Mitragotri, S. Elasticity of Nanoparticles Influences Their Blood Circulation, Phagocytosis, Endocytosis, and Targeting. *ACS Nano* **2015**, *9*, 3169−3177.
(49) Jokerst, J. V.; Lobovkina, T.; Zare, R. N.; Gambhir, S. S. Nanoparticle Pegylation for Imaging and Therapy. *Nanomedicine* **2011**, *6*, 715−728.
(50) Albanese, A.; Tang, P. S.; Chan, W. C. The Effect of Nanoparticle Size, Shape, and Surface Chemistry on Biological Systems. *Annu. Rev. Biomed. Eng.* **2012**, *14*, 1−16.
(51) Febvay, S.; Marini, D. M.; Belcher, A. M.; Clapham, D. E. Targeted Cytosolic Delivery of Cell-Impermeable Compounds by Nanoparticle-Mediated, Light-Triggered Endosome Disruption. *Nano Lett.* **2010**, *10*, 2211−2219.
(52) Cheng, T. L.; Wu, P. Y.; Wu, M. F.; Chern, J. W.; Roffler, S. R. Accelerated Clearance of Polyethylene Glycol-Modified Proteins by Anti-Polyethylene Glycol IgM. *Bioconjugate Chem.* **1999**, *10*, 520−528.
(53) Lu, D.; Zhang, H. F.; Ludwig, D.; Persaud, A.; Jimenez, X.; Burtrum, D.; Balderes, P.; Liu, M. L.; Bohlen, P.; Witte, L.; Zhu, Z. P. Simultaneous Blockade of Both the Epidermal Growth Factor Receptor and the Insulin-Like Growth Factor Receptor Signaling Pathways in Cancer Cells with a Fully Human Recombinant Bispecific Antibody. *J. Biol. Chem.* **2004**, *279*, 2856−2865.
(54) Cheng, T. L.; Chou, W. C.; Chen, B. M.; Chern, J. W.; Roffler, S. R. Characterization of an Antineoplastic Glucuronide Prodrug. *Biochem. Pharmacol.* **1999**, *58*, 325−328.
(55) Shahied, L. S.; Tang, Y.; Alpaugh, R. K.; Somer, R.; Greenspon, D.; Weiner, L. M. Bispecific Minibodies Targeting HER2/Neu and CD16 Exhibit Improved Tumor Lysis When Placed in a Divalent Tumor Antigen Binding Format. *J. Biol. Chem.* **2004**, *279*, 53907−53914.
(56) Chen, K. C.; Cheng, T. L.; Leu, Y. L.; Prijovich, Z. M.; Chuang, C. H.; Chen, B. M.; Roffler, S. R. Membrane-Localized Activation of Glucuronide Prodrugs by Beta-Glucuronidase Enzymes. *Cancer Gene Ther.* **2007**, *14*, 187−200.
(57) Wu, C. H.; Balasubramanian, W. R.; Ko, Y. P.; Hsu, G.; Chang, S. E.; Prijovich, Z. M.; Chen, K. C.; Roffler, S. R. A Simple Method for the Production of Recombinant Proteins from Mammalian Cells. *Biotechnol. Appl. Biochem.* **2004**, *40*, 167−172.
(58) Iyer, A. K.; Su, Y.; Feng, J.; Lan, X.; Zhu, X.; Liu, Y.; Gao, D.; Seo, Y.; Vanbrocklin, H. F.; Courtney Broaddus, V.; Liu, B.; He, J. The Effect of Internalizing Human Single Chain Antibody Fragment on Liposome Targeting to Epithelioid and Sarcomatoid Mesothelioma. *Biomaterials* **2011**, *32*, 2605−2613.
(59) Bartlett, G. R. Phosphorus Assay in Column Chromatography. *J. Biol. Chem.* **1959**, *234*, 466−468.
(60) Sun, J. S.; Zhang, L.; Wang, J. L.; Feng, Q.; Liu, D. B.; Yin, Q. F.; Xu, D. Y.; Wei, Y. J.; Ding, B. Q.; Shi, X. H.; Jiang, X. Y. Tunable Rigidity of (Polymeric Core)-(Lipid Shell) Nanoparticles for Regulated Cellular Uptake. *Adv. Mater.* **2015**, *27*, 1402−1407.

DOI: 10.1021/acsnano.5b05661
ACS Nano 2016, 10, 648−662